Soft Matter

Cite this: *Soft Matter*, 2012, **8**, 10868

www.rsc.org/softmatter

PAPER

An amphiphilic silicone-modified polysaccharide molecular hybrid with *in situ* forming of hierarchical superporous architecture upon swelling†

Wei-Chen Huang, San-Yuan Chen* and Dean-Mo Liu*

Received 12th June 2012, Accepted 21st August 2012
DOI: 10.1039/c2sm26361k

Most hydrogels face the challenge that extensive water uptake deteriorates their mechanical integrity, which restricts potential uses and, in some cases, reduces therapeutic performance in biomedical applications. Motivated by the concept that structural optimization was able to improve the mechanical properties whilst maintaining a high water uptake, in this work we designed a new type of strong network, *i.e.* PDMS-crosslinked-NOCC polymer networks (PMSC CAPNs), by esterification between cross-linked PDMS diol (bis(hydroxyalkyl) terminated polydimethylsiloxane, silicone) and NOCC (*N*,*O*-carboxymethyl chitosan). By manipulating the cross-linked density with PDMS, a hierarchical structure in which PDMS-rich microgels were randomly distributed within the underlying PMSC hydrogel could be tailored through the control of polymer–polymer and polymer–solvent interactions. Besides, the resulting hybrid hydrogel displayed an efficient self-foaming capability to create *in situ* a hierarchical superporous microarchitecture upon swelling. The swelling behavior accounted for by Flory–Rehner theory indicated that the PDMS macromonomeric crosslinker not only caused the development of a superporous microarchitecture under solvation effects but also escalated both strength and elasticity to the final hydrogel. A new swelling model based on spectroscopic examination of the PMSC CAPNs was successfully proposed, which nicely defined the unique structural transition of the hydrogel upon swelling. We also envision the potential development of such a hybrid hydrogel for advanced biomedical applications.

Introduction

Hydrogels are polymeric cross-linked materials that can be considered as a viscoelastic entity with excellent water-absorbing capabilities. Along with structural sustainability, mechanical flexibility and peculiar softness, hydrogels have attracted considerable attention for a variety of biomedical applications such as tissue engineering, intelligent drug delivery systems, wound dressing, contact lenses, biosensors, enzymatic catalysis supports, and bio-adhesives, *etc.*[1,2] Recently, Calvert[3] indicated that by reinforcing the molecular structures, the integrity and the cross-linking density of the hydrogels can be greatly improved in turn, allowing the design of soft biomimetic machines. For this reason, numerous efforts have been devoted to explore novel methods of controlling or upgrading the architecture of hydrogels.[4] For example, Gong *et al.* synthesized a double-network (DN) structure, which can sustain a compressive pressure as high as several tens of MPa. Such a structure imparts brittle and rigid properties suitable for the use of gel-based cartilage as a strong support.[5] Hu *et al.* designed a two-phase microgel-embedded hydrogel film with good performance on elongation, while its excellent toughness stands a good chance of making it applicable for tissue scaffolds.[6] Unfortunately, the high water content usually deteriorates the mechanical integrity of hydrogels, degrading their therapeutic performance and therefore restricting possible applications, especially for the design of a biomimetic membrane or wound dressings, since they require not only high water-absorbing ability for extensive exudation but a reinforced toughness for skin replacement.[7,8] However, optimization toward the membranes for better superabsorbent ability, strength, and elasticity simultaneously, through the development of flexible superporous micro-architectures,[9] has rarely been reported.

Because of the unique behavior of self-assembly in various solvents, covalently crosslinked amphiphilic polymer networks (CAPNs) are considered to be a good candidate as the structure-reinforced gel designed for advanced bio-adhesive membranes.[10–12] Since the formation of CAPNs is attributable to the chemical cross-links between both hydrophilic and hydrophobic polymers, CAPNs exhibit dual characteristics of two constituting polymers with strong covalent bonds. Note that

Department of Materials Science and Engineering, National Chiao Tung University, HsinChu City, 30010, Taiwan. E-mail: sanyuanchen@mail.nctu.edu.tw; deanmo_liu@yahoo.ca; Fax: +886 3 5724727; Tel: +886 3 5712121 ext. 31818 and 55391

† Electronic supplementary information (ESI) available: Esterification process of PMSC; FTIR spectra of NOCC, PMSC-1, PMSC-2, and PMSC-3; X-ray diffraction patterns of NOCC, PMSC-1, PMSC-2, and PMSC-3. See DOI: 10.1039/c2sm26361k

CAPNs form nanophase- or microphase-reinforced hydrogels in a single system by self-assembly, rather than by incorporating an additional phase by two-system embedding, thus providing a low-energy route for the formation of a hierarchical structure with beneficial mechanical properties. Besides, unlike homopolymer gels, CAPNs are able to swell in both polar and nonpolar solvents due to their amphiphilic nature, which is advantageous for use in both hydrophilic and hydrophobic drug delivery.[13]

In this work, we developed an unprecedented type of amphiphilic, zwitterionic, and strong polymer network, *i.e.* PDMS-crosslinked-NOCC amphiphilic polymer networks (PMSC CAPNs), by esterification between cross-linked PDMS diol [bis(hydroxyalkyl) terminated polydimethylsiloxane, silicone] and NOCC (*N*,*O*-carboxymethyl chitosan). NOCC, which is highly water-absorptive and water-retentive in neutral conditions, has been reported to help wound healing and scar prevention by promoting skin fibroblast proliferation and inhibiting keloid fibroblast proliferation.[14,15] On the other hand, PDMS, which has been widely used in medical applications because of its biocompatibility, high water and oxygen permeability, low flammability and good oxidative stability,[16,17] was generally implemented as artificial skin. By chemically cross-linking hydrophilic NOCC with hydrophobic PDMS, the resulting PMSC CAPNs maintain excellent hydrophilicity together with reinforcement of flexibility during swelling by both microgel- and fiber-reinforcement due to the micro-phase separation. In addition, by controlling the cross-linked density with PDMS involving polymer–polymer and polymer–solvent interactions, a hierarchical structure can be tailored. A new swelling model based on spectroscopic examination of the PMSC CAPNs was successfully proposed to define the unique structural transition of the hydrogel upon swelling. It is concluded that by combining zwitterionic polysaccharide and elastic silicone, potential biomedical products of the soft biomimetic membrane such as the dermis, cornea, and/or arterial skin, are foreseen in the future.

Materials and methods

Materials

Chitosan (M_w = 260 000 g mol^{-1}, deacetylation degree = 80%, insoluble impurity k < 1%), and bis(hydroxyalkyl) terminated polydimethylsiloxane (PDMS diol, M_w = 5600 g mol^{-1}), were both purchased from Sigma-Aldrich and used as received without further purification.

Preparation of polydimethylsiloxane-modified chitosan

The polydimethylsiloxane-modified chitosan (PMSC) copolymer was prepared by a two-step synthesis: carboxymethylation and esterification. In the first step, NOCC was synthesized by grafting carboxymethyl groups onto the amino site (N-site) and the hydroxyl site (O-site) of pristine chitosan.[18] Briefly, 5 g chitosan was suspended in 2-propanol (50 ml) at room temperature while being stirred for 30 min. The resulting suspension was gently mixed with 12.5 ml NaOH solution. The mixture containing 13.3 M NaOH was mixed with 25 g chloroacetic acid to prepare a carboxymethyl chitosan sample with a high degree of carboxymethyl substitution. After NOCC was obtained, 2 g of the dried sample was dissolved in distilled water (50 ml) and stirred for 24 h. The resulting solutions were mixed with methanol (50 ml), then stirred vigorously for 4 h, and followed by adding bis(hydroxyalkyl) terminated polydimethylsiloxane, which was dispersed in 2-propanol as a solution (50% v/v) in advance, at PDMS : NOCC molar ratios of 25 : 1, 50 : 1 and 100 : l, represented as low, medium and high grafting ratios, and designated as PMSC-1, PMSC-2 and PMSC-3 respectively. Following catalysis with sulfuric acid, after the mixture was maintained and reacted at 60 °C for 24 h to be esterified, the resulting solution was dialyzed by using a dialysis tubing cellulose membrane (M_w cut-off 12 400 g mol^{-1}, average flat width 33 mm) with ethanol/diethyl ether (9 : 1 (v/v)) for 1 day. After repeating dialysis 3 times, the purified product was obtained after drying at 50 °C overnight.

Characterization of polydimethylsiloxane-modified chitosan

NMR and infrared spectroscopy techniques were used to characterize PMSC. ^{1}H NMR was performed on a 500 MHz VARIAN UNITY INOVA NMR spectrometer and revealed the chemical structures of PMSC, NOCC, and PDMS by using D_2O (for PMSC and NOCC) and deuterated chloroform ($CDCl_3$, for PDMS) as solvents. The chemical shift at 1.9 ppm was taken as a reference to normalize the calculation of the integration areas. For infrared spectroscopic analysis (FTIR), a dried sample of 5 mg, which was mixed with 300 mg dry KBr, was pressed into a pellet using a macro KBr die kit. A FTIR spectrum of 50 scans at 4 cm^{-1} resolution was obtained by using a spectrum 100 FTIR spectrometer (PerkinElmer Inc.). Small-angle X-ray scattering (SAXS) measurements were carried out on a Simultaneous SAXS setup with a monochrome beam BL23A1 at the National Synchrotron Radiation Research Center (NSRRC). The colloidal dispersions in 1% water solution were directly placed into the capillary sample holders. The distance from sample to detector was 975 mm and the beam stop was a molybdenum disk of diameter 4 mm. The data was collected using a one-dimensional position-sensitive detector, which was calibrated with a Fe55 source. Moreover, the 1% colloidal solution at different pH values was characterized by using electrophoretic light scattering (ELS) for zeta potential determination. Briefly, a 10 mg mL^{-1} PMSC sample was suspended in distilled water under gentle shaking at 25 °C for 24 h, followed by ultrasonication using a probe type sonifier (Automatic Ultrasonic Processor UH-500A, China) at 30 W for 2 min. The sonication was repeated three times to get a semi-turbid solution. To inhibit the heat buildup during sonication, the pulse function was used (pulse on 5.0 s; pulse off 1.0 s). All measurements were done with a wavelength of 633.0 nm at 25 °C with an angle detection of 90°. Each sample was repeatedly measured three times. X-Ray diffraction (XRD) profiles were collected with a Bruker D2 diffractometer using Nickel-filtered Cu-Kα radiation (k = 0.15406 nm) and scanned from 5° to 60° at a scan speed of 3° per min.

Preparation and characterization of the hydrogel

The PMSC hybrid hydrogels were prepared by casting 10 g water solution at the concentration of 1 wt% onto a dish of 3 cm in diameter, followed by incubating at 50 °C for 1 day. The

appearance of thin-film hydrogels was fabricated on a glass slide and observed by optical microscopy. To observe the change in appearance and morphology of the hydrogels during swelling, fluorescence-labeled hydrogels, which were examined by confocal microscopy (Axiovert 100M), were obtained by coupling PMSC with FITC (fluorescein isothiocyanate), where the isothiocyanate reactive group is reactive towards the amine groups on the backbone of PMSC. Briefly, 1 mg FITC and 100 mg PMSC colloidal solution were dissolved in 10 ml deionized water. After stirring vigorously for 4 h, the solution was coated onto a glass slide by spin-coating; then it could form a layer of film-like hydrogel after being dried at 50 °C for 8 h. The specimen of swollen hydrogels, which needed to be wetted slightly, was moistened with a sprayer and examined by fluorescence microscopy. Then the analysis was carried out after dehydration by the freeze-drying method. Additionally, Scanning Electron Microscopy (JEOL 6700, Japan) was applied to obtain the cross-section view of the dehydrated samples.

The swelling ratio of the hydrogels was estimated by measuring the change in sample weight before and after immersion in deionized water. The procedure was repeated five times. The swelling ratio was determined according to the following equation:

$$\text{Swelling ratio, SR} = \frac{W_s - W_d}{W_d} \times 100\% \quad (1)$$

where W_s and W_d represent the weights of the swollen and dried samples, respectively. All the results are obtained by averaging the five measurements. The measurement error is estimated to be <3%. The wetting ability was examined using the water contact angle, which was measured with a VCA Optima contact angle (CA) analyzer with an average of five measurements. The tensile test was performed on the as-prepared hydrogels with a commercial test machine (MTS Tytron 250). In order to obtain hydrogels with the same swelling ratio, each dry sample, which was cut into a dog-bone shape of 3 cm in length and 1 cm in width, was set in a steam bath in the same closed system with water of 60 °C for 10–15 minutes. Depending on the different samples, the measured weight was used to decide the bath duration for the same swelling ratios of 0%, 50%, 100%, and 150%. After swelling, each sample was directly set onto the gauge with an initial length of 1 cm. With a working rate of 0.2 mm s^{-1}, the fracture stress σ and fracture strain ε were derived at breaking point.

Results and discussion

Preparation and characteristics of PMSC hydrogels

Poly(dimethylsiloxane)-crosslinked-carboxymethyl chitosan (PMSC) was synthesized *via* an esterification reaction between the carboxylic groups of NOCC and the hydroxyl groups of PDMS, where the release of a water molecule, as a result of the interaction between –OH of the carboxylic acid groups and –H of the hydroxyl groups, ensured the formation of an ester bond between NOCC and PDMS. The resulting FTIR spectra in Fig. S1 and S2 (ESI†) show the disappearance of the characteristic band (1749 cm^{-1}) of the carboxylic acid of NOCC, confirming the designated esterification reaction. The grafting ratio in the resulting co-polymer can be quantitatively determined using the integration area of the peaks from the ^{1}H NMR spectra. For NOCC, shown in Fig. 1a, the chemical shifts at 1.9 and 3.1 ppm were assigned to the protons on the acetyl group and at the C2 position (H-2), respectively. The ring protons (H-3 to H-6) were considered to resonate at 3.5–4.0 ppm. The chemical shifts at 3.9 and 4.2 ppm were designated to the protons of OCH_2CO (O-position) and NCH_2CO (N-position) of NOCC, respectively.[19] After the reaction occurred, Fig. 1b indicates additional chemical shifts at 0.1 ppm (Si–CH_3, α), 0.43 ppm (–Si–CH_2CH_2–, β), 1.6 ppm (–$CH_2CH_2CH_2$–, γ), and 3.6 ppm (–OCH_2CH_2–, δ), which correspond to methyl protons along the backbone of PDMS. Thus, the degree of esterification (DE), which is represented by the ratio of –COOR to –COOH, *i.e.* the amount of –COOH that reacted with the –OH of PDMS, was obtained by calculating the degree of carboxymethyl substitution of NOCC and PMSC:

$$\text{DE} = 1 - \left[\frac{(\text{area}_{3.9\ \text{ppm}} + \text{area}_{4.2\ \text{ppm}})_{\text{PMSC}}}{(\text{area}_{3.9\ \text{ppm}} + \text{area}_{4.2\ \text{ppm}})_{\text{NOCC}}}\right] \quad (2)$$

Thus the DE value was determined as 0.39, 0.51 and 0.61 for the samples of PMSC-1, PMSC-2, and PMSC-3, respectively, indicating that the grafting ratio increased with the addition of PDMS.

As the CAPNs evolved, in Scheme 1, the PDMS diol (colored brown), plays the role of a hydrophobic bridge, which provided a connection between hydrophilic NOCC polymer chains (colored red) by covalent bonding. According to the colloid behavior, there are two driving forces, the solvation effect and the salt ion effect, leading to the formation of PMSC hydrogels. Fig. S3† exhibits the schematic process of the formation of PMSC

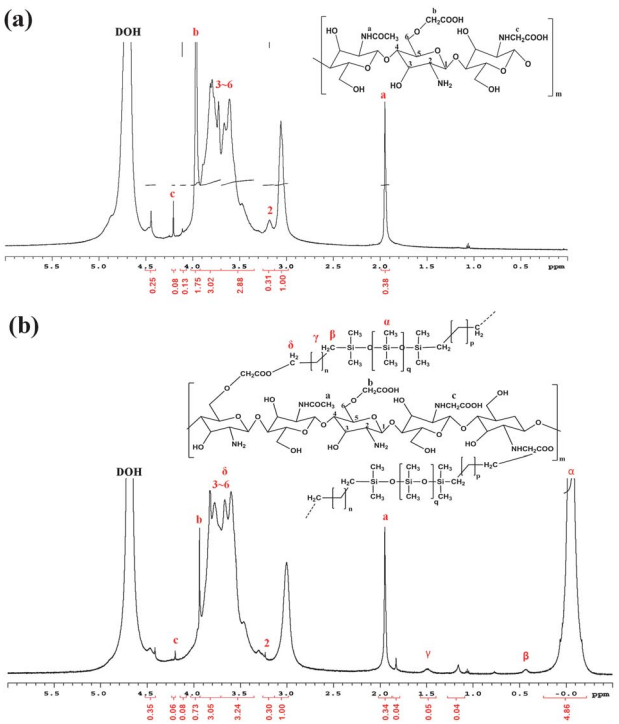

Fig. 1 ^{1}H NMR spectra of (a) NOCC and (b) PMSC in D_2O.

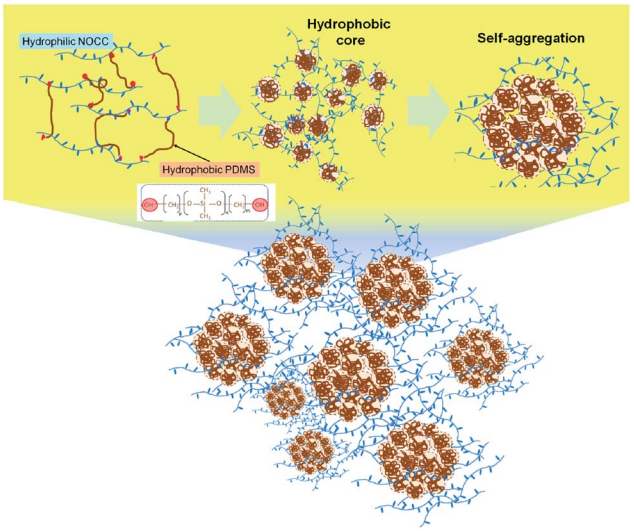

Scheme 1 Schematic drawing of the aggregation of PMSC APCNs.

hydrogels. Owing to the solvation effect, the hydrophobic groups of the CAPNs tend to coil together in order to avoid unfavorable contact with the water.[20] Similarly, in the PMSC hydrogels, the molecular chains of polysiloxane were able to aggregate into a hydrophobic core. Then, as a result of thermodynamically favorable stabilization,[21] the suspensions existed with a hierarchical architecture, inside which the secondary micro-domains (*i.e.* hydrophobic PDMS-rich aggregations) were formed between hydrophilic NOCC-rich networks. Continuously, during the drying process, the decrease of water raised the concentration of the PMSC solution so that the second driving force, the salt ion effect, arising from the $-NH_2^+$ and $-COO^-$ of NOCC becomes stronger. Based on the DLVO theory, when the salt ion content is high enough, the attractive van der Waals forces will overcome the charge repulsion so that the PMSC aggregations get closer. Thus, the dried hierarchical PMSC hydrogel (*i.e.* xerogel) with the microgels compactly cross-linked within bulk networks was finally formed (Fig. S3).†

The FITC-PMSC image in Fig. 2a clearly indicates the presence of numerous spherical microgels with a size range of 1–5 micrometers in diameter, which were immobilized within the network structure of the PMSC hydrogel. To further explore the underlying micro-structural development, the freeze-drying method was employed to dehydrate the swollen hydrogels in order for the swollen structure to stay in place upon further examination.

It was found that the immobilized microgels (dark spherical spots) were swollen extensively in the hydrogels in Fig. 2b. The microgels evolved into a highly porous architecture upon swelling, with different microstructural morphology compared with the underlying network structure, wherein the latter showed a fibrous-like architecture, whilst the former displayed a polygonal construct. Such a porosity development is assumed to be the result of self-aggregation of the hydrophobic PDMS-rich units. A plausible explanation is illustrated in Scheme 1, in which the microgel region is virtually a PDMS-rich counterpart of the resulting hydrogel and form a more compact aggregation expected upon swelling, whilst the underlying network is a

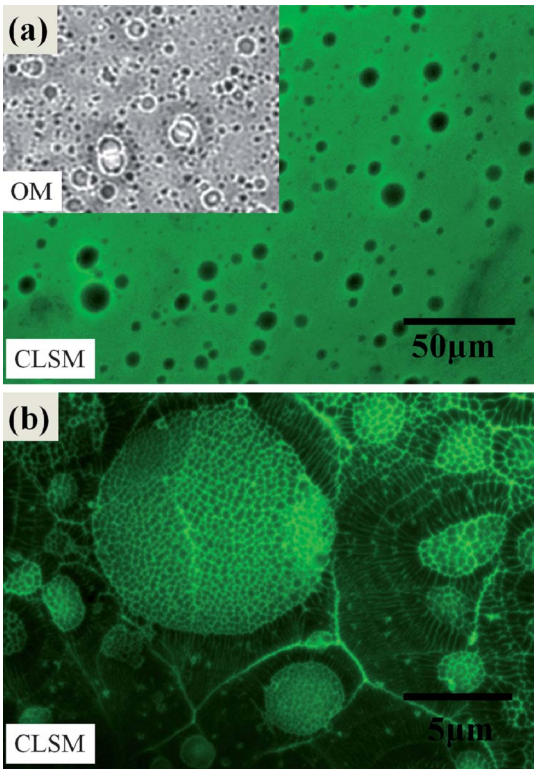

Fig. 2 OM and CLSM images of dried samples: (a) PMSC hydrogels, and (b) freeze-dried swollen PMSC hydrogels.

PDMS-poor region, where extensive swelling associated with poorer aggregation gave rise to a more porous architecture with a fibrous construction.

Fig. 3a shows a plot of the scattering intensity ($I(Q)$) of Small Angle X-ray Scattering (SAXS), *versus* the scattering vector (Q) of 1 wt% NOCC, PMSC-1, PMSC-2, and PMSC-3 in DI water. In the SAXS spectrum, the low-Q scattering region ($Q < 0.03$) indicated the long-range spatial arrangement and the high-Q scattering region ($Q > 0.03$) represented the short-range interaction, *i.e.* the geometry of the cluster. In the low-Q region, it was found that the intensity of CAPNs, *e.g.* PMSC-1, PMSC-2, and PMSC-3, was higher than that of NOCC, suggesting a higher compact density of cross-linked hydrogels. On the other hand, the high-Q region ($Q > 0.03$) showed that PMSC-1, PMSC-2, and PMSC-3 had steeper profiles than NOCC, indicating that PMSC-1, PMSC-2, and PMSC-3 had a different degree of solvation from NOCC, *e.g.* clusters formed. To analyze the inter-molecular and intra-molecular interaction of CAPNs, the following formula derived by Hammouda *et al.*[22] was used to fit the scattering intensity from SAXS to systems of diverse or micro-phase separation such as polyelectrolyte solutions, block copolymers and self-assembled systems:

$$I(Q) = \frac{A}{Q^n} + \frac{C}{1 + (QL)^m} + B \quad (3)$$

where A, C and B represent a Q-independent background. The first term A/Q^n can be qualitatively homologous Porod-like scattering, and exponent n can be obtained by linearly fitting the strength of the long-range scattering.

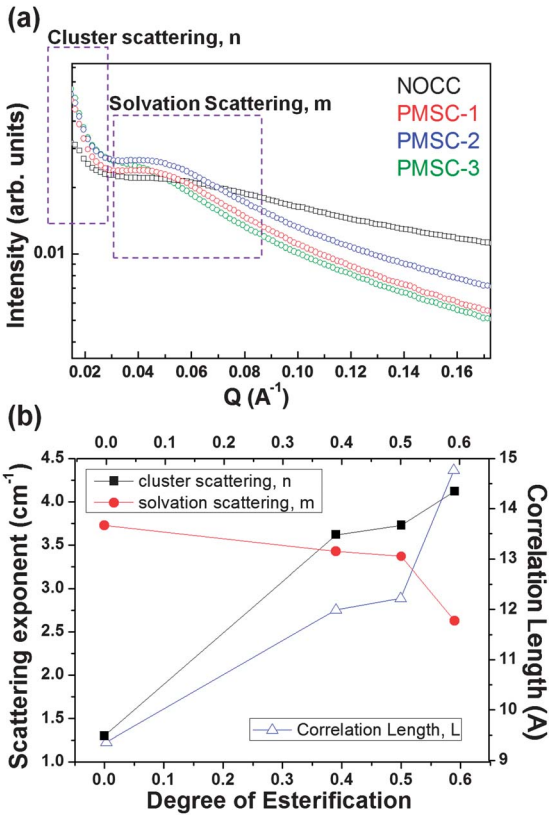

Fig. 3 (a) SAXS analysis of 1% NOCC, PMSC-1, PMSC-2, and PMSC-2 polymers in deionized water; (b) variation of the fitting results from SAXS shown by cluster scattering, n, solvation scattering m, and correlation length L.

The first term is usually used for the arrangement of a cluster or a large gel network. A larger value of n indicates a higher density of the compact networks. The second term $C/[1 + (QL)^m]$, which represents the short-range behavior, gives the expression of high-Q scattering for the interactions of the solvent–polymer chains. By non-linear fitting with a Lorentzian function, the exponent m, which stands for the degree of solvaphilicity, and a correlation length L, representing the size of the cluster, can be obtained.

As shown in Fig. 3b, it was found that in the low-Q range ($Q <$ 0.03), the n values increased from 1.30, 3.62, 3.73, to 4.12 with the increase in the DE (degree of esterification) value from 0, 0.39, 0.51, to 0.61, respectively. Since the previous studies indicated that mass fractal scattering will occur in the range 1 to 3, it suggests that the amphiphilic PMSC exhibited a stronger tendency to form fractal architecture in the water solution, which was experimentally confirmed as aforementioned.[23]

For the high-Q regime, the scattering exponent m was determined to be 3.43, 3.37, 3.16 and 2.63 for NOCC, PMSC-1, PMSC-2, and PMSC-3, respectively. The decreasing m values with increasing PDMS addition implied a decrease in the hydrophilic effect.[21] The substitution of PDMS leads to the elimination of –COOH groups whose ionized status ($–COO^-$) will enhance the electrostatic interaction and the hydration reaction. Verified by electrophoretic light scattering (ELS) shown in Fig. 4, the variation in zeta potential for NOCC, PMSC-1,

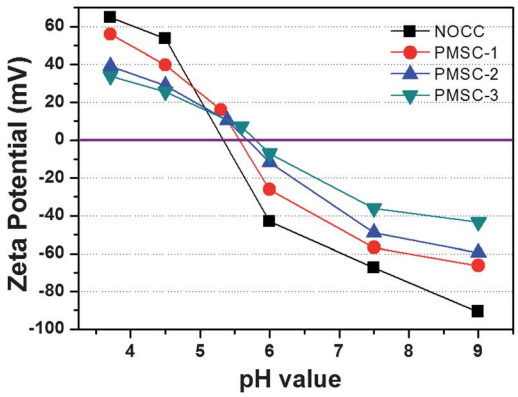

Fig. 4 Zeta potential of NOCC, PMSC-1, PMSC-2, and PMSC-3 at different pH values.

PMSC-2, and PMSC-3 demonstrates that with increased PDMS grafting, the PMSC samples became less ionizable for the pH range under study, which was accompanied by a reduction in the electrolytic potency. Therefore, in DI water, the hydrophobicity brought out the formation of a PDMS hydrophobic core with a measured zeta potential of +64.7 mV, +16.0 mV, +10.4 mV, and +7.1 mV for NOCC, PMSC-1, PMSC-2, and PMSC-3, respectively, indicating that more PDMS grafting leads to a weaker repulsive force between nearby hydrophobic cores. As a result, the basic unit cores with a smaller repulsive force got so much closer that final aggregations with a larger size were formed. As illustrated in Fig. 3b, the correlation length, L, which represents the size of the core formed by the hydrophobic interactions increased from 9.37 Å, 11.86 Å, 12.22 Å, to 14.76 Å for NOCC, PMSC-1, PMSC-2, and PMSC-3, respectively.

Meanwhile, for a given solvent quality, the volume of an aggregated microgel can be estimated:[24]

$$R_{\text{microgel}} \sim (N_p)^{\nu} C_{pp}^{1/3-\nu} (h^*)^{1/5} \quad (4)$$

where N_p is the length of the hydrophobic segment, C_{pp} is the average number of cross-linked points per hydrophobic segment, h^* is the optimal size of the unit core, and ν is 1/2 in θ-solvent and 3/5 in a good solvent. From the SAXS analysis, it was demonstrated that with increased PDMS grafting (higher DE value), an increase in the n and L values, which represent the cross-linking density C_{pp} and the size of the basic unit core h^*, respectively, will lead to a larger size of the microgels. This argument was further supported from the OM images in Fig. 5, where the PMSC hydrogels with higher DE value depicted an increasing size and number of microgels from PMSC-1 to PMSC-2 to PMSC-3, indicating that the size of the self-aggregated microgels increased with increasing PDMS grafting.

Swelling mechanism of PMSC

Fig. 6a illustrates the plots of swelling time *versus* swelling ratio of the NOCC, PMSC-1, PMSC-2, and PMSC-3 hydrogels in DI water for 24 hours. The swelling profiles show that the swollen NOCC hydrogels tended to collapse within a short period of time, *i.e.*, less than 10 minutes. However, by cross-linking with PDMS, PMSC showed a prolonged swelling behavior over a

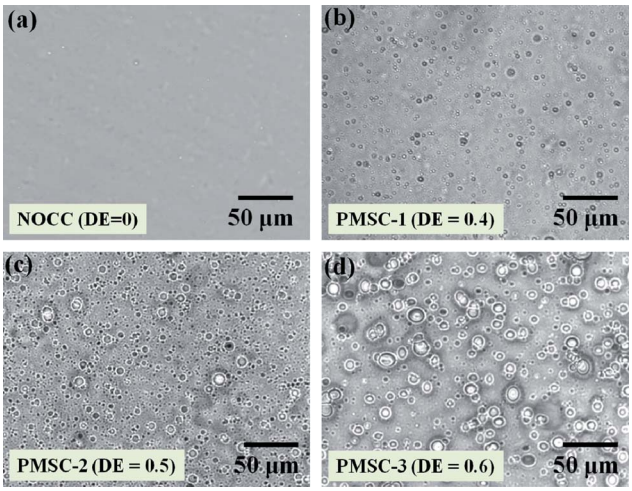

Fig. 5 OM images of dried samples with different degrees of esterification (DE): (a) NOCC (DE = 0), (b) PMSC-1 (DE = 0.4), (c) PMSC-2 (DE = 0.5), and (d) PMSC-3 (DE = 0.6) hydrogels.

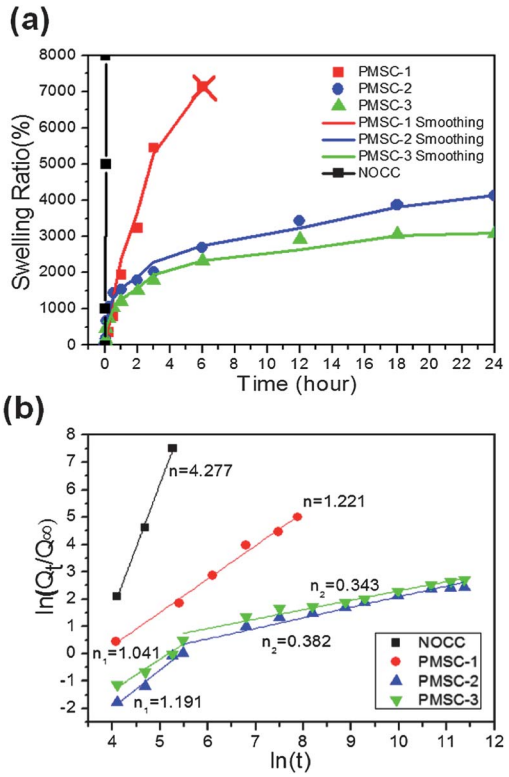

Fig. 6 (a) Swelling profiles of NOCC, PMSC-1, PMSC-2, and PMSC-3 hydrogels. (b) A plot of $\ln(Q_t/Q_\infty)$ *versus* $\ln(t)$ of data from (a).

relatively long time period. Among the samples, PMSC-1 was found to swell extensively until reaching a structural collapse, but the structural integrity has been maintained over a prolonged time for 6 hours. Such a structural failure resulted from the insufficient cross-linking density. However, PMSC-2 and PMSC-3 can achieve a swelling equilibrium state (3000–4000%) with structural integrity but became too fragile within 36 and 24 hours, respectively. (Their appearance is shown in Fig. S5a.†) In order to investigate the swelling kinetics of PMSC, an empirical relation, eqn (5), was used to determine the swelling mechanism:[25]

$$\ln\left(\frac{Q_t}{Q_\infty}\right) = \ln(k) + n\ln(t) \quad (5)$$

where Q_t and Q_∞ are the mol% sorption at time t and at equilibrium, respectively, k is a constant that depends on the structural characteristics of the polymer and n is the diffusion exponent, which is related to the absorption mechanism. Therefore, the derived n can be used to determine the contribution of the structural limit or the diffusion limit. If $n = 0.5$, Fickian diffusion occurs, indicating that the rate of molecular diffusion is much less than the mobility of the polymer segment. If n approaches 1.0, the mechanism of sorption will be non-Fickian, meaning the diffusion rate of permeant molecules is faster than the mobility of the polymer segment. By regression analysis of the kinetic parameters, n can be obtained from the slope of the plot of $\ln(Q_t/Q_\infty)$ *versus* $\ln(t)$ in Fig. 6b. For NOCC, n is 4.277, which was un-identifiable because the structure collapsed suddenly. For PMSC-1, $n = 1.221$ was determined but the hydrogel structure still collapsed in about 6 h. However, with increasing PDMS modification, PMSC-2 and PMSC-3 demonstrated two-stage swelling behavior. In the earlier stage, the n values of PMSC-2 and PMSC-3 were calculated to be 1.191 and 1.041, respectively, indicating a swelling control model, *i.e.* the rate of polymer relaxation was slower than the water diffusion. However, in the later stage of swelling, a turning point was seen, with the n values changing to 0.382 and 0.343 for PMSC-2 and PMSC-3, respectively, indicating that Fickian-diffusion dominated the swelling behavior.

PDMS effect on the swelling

To probe the swelling behavior of PMSC hydrogels, it is important to investigate polymer–polymer and polymer–solvent interactions upon hydrogel transition from the dried to the swollen state. By quoting Flory–Rehner theory, a polyelectrolyte hydrogel reaches its swelling equilibrium at the balance of the pressures coming from the osmotic pressure, which is generated as the sum of the mixing phase (π_{mix}) of the polymer–solvent interaction, the electrostatic interaction (π_{ion}) of the ionized groups or ionized groups/surrounding solvent, and an elastic force (π_{elast}) due to the polymer–polymer interaction. In general, the swelling tendency of the hydrogels can be explained by:[26]

$$\pi_{final} = \pi_{mix} + \pi_{ion} + \pi_{elast} \quad (6)$$

where π_{ion} represents the expansive pressure generated by the charged groups. It can be deduced that the variation in π_{ion}, π_{elast}, and π_{mix} will result in a final balanced driving osmotic pressure π_{final} to encourage swelling.

π_{mix} is generated by the chemical potential arising from contact of the pure solvent with an initially pure, amorphous, unstrained gel network, which can be exhibited in the wetting ability between hydrogels and water. A good wetting ability, *i.e.* hydrophilicity, will generate a π_{mix} to assist water diffusion into the networks, while hydrophobicity will cause a decrease in affinity (*i.e.* lower π_{mix}) to water. Due to the closely packed methyl groups around the backbone of polysiloxane, PDMS has

a small surface tension of 20.4 mN m^{-1}, which makes it too hydrophobic to be wetted.[27] Hence, hydrogels cross-linked by non-polar PDMS will deteriorate their wetting ability. This was verified by the contact angle analysis, where the contact angles of NOCC, PMSC-1, PMSC-2, and PMSC-3 were 53.2°, 72.9°, 91.9°, and 97.1°, respectively. The results indicated that the addition of PDMS reduced wetting ability and led to the decrease of π_{mix}, so the water uptake into the hydrogels was inhibited. Therefore, the increased hydrophobic effect may reduce the swelling rate of the hydrogels.

For NOCC or PMSC copolymer, it is a polyelectrolyte whose amine groups ($-NH_2$) and carboxylic groups (–COOH) are ionizable in water solution.[28] A π_{ion} value can be generated by the electrostatic interaction and the hydration reaction between the ionized chains and water. Referring to the aforementioned results of the zeta potential in 3–1 (shown in Fig. 4), the electrolytic potency of the hydrogel was reduced by incorporating PDMS. A reduction in π_{ion} is then expected.

An elastic response of the network acts as a solvent potential barrier, which in turn decreases π_{elast}. Incorporation of the cross linking agent, PDMS, increases the elasticity of the semi-crystalline NOCC.[29] The crystallinity of PMSC decreased proportionally with the increasing cross-linking ratio of PDMS, as evidenced by XRD analysis (Fig. S4†). The (110) diffraction peak of NOCC at 19.3° became increasingly weaker and broader from PMSC-1 to PMSC-2 to PMSC-3.[30] Moreover, the diffraction peak at $2\theta = 19.3°$, shifted to higher scattering angle of about $2\theta = 24°$, indicated partial rearrangement of the polysaccharidic chain occurring as a result of chemical modification.

In addition, to further provide direct evidence of the PDMS effect on the π_{elast} values of swollen hydrogels, the measurement of elongation and tensile strength with different swelling ratios is able to provide a strong indication of the mechanical properties of polymer chains. Fig. 7(a) and (b) depict the fracture strain ε and the fracture stress (tensile stress) σ, which were derived from the PMSC-1, PMSC-2, and PMSC-3 hydrogels with swelling ratios of 0%, 50%, 100%, 150% and 250%. For the dried samples, the fracture strain ε and fracture stress σ, *i.e.* (ε, σ), of PMSC-1, PMSC-2, and PMSC-3 were measured to be (0.105, 26 MPa), (0.065, 26.7 MPa), and (0.05, 27 MPa), respectively, where no appreciable difference was detected among them. With the increase of the swelling ratio, the fracture strain ε of all samples increased while the fracture stress decreased sharply. It means that the water intake not only led to relaxation of the polymer but also gave additional free volume for polymer movement. So the relaxation of the networks led to an increase in elasticity. At the same time, from the comparison between PMSC-1 and PMSC-2, it was found that more cross-linking with PDMS led to a higher strain being observed over the same swelling ratio (Fig. 7a). Since the functionality of the cross-links depends on their chemical nature, PDMS, a polysiloxane, has the most open structure with the flattest angle and the longest bond length, and will impart good elasticity to prevent networks from collapsing.[27] Hence, as the swelling ratio increased, especially after the relaxation of the PDMS-rich microgels, the stretched PMSC polymer chains generated elasticity to restrict water diffusion, which resulted in a reduction in π_{elast}.

It was interesting to find that PMSC-3 was found to be more brittle than PMSC-2 due to its lower strain and higher stress, as

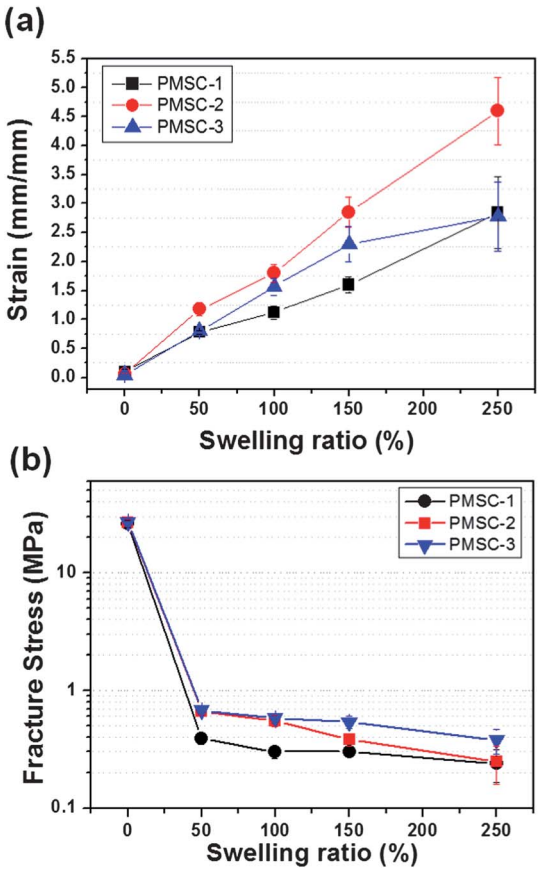

Fig. 7 Tensile properties of the NOCC, PMSC-1, PMSC-2, and PMSC-3 hydrogels measured at swelling ratios of 0%, 50%, 100%, 150% and 250%. (a) Representative strain–swelling curve; (b) representative stress–swelling curve.

depicted in Fig. 7a and b. This was explained by comparison of the microstructures, shown in the SEM images in Fig. 8a–d, and it demonstrated the distinct porous structure between four samples at 100% swelling. In Fig. 8a, *i.e.* NOCC, the pore size of

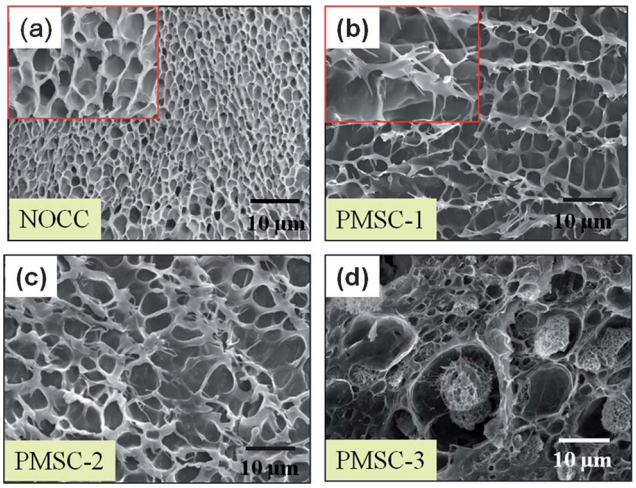

Fig. 8 Cross-section view of SEM images of swollen hydrogels: (a) NOCC; (b) PMSC-1; (c) PMSC-2; (d) PMSC-3.

the deformed networks was observed to be 1 μm in size, whilst the wall thickness was about 100 nm in width. In contrast, for PMSC-1 (DE = 0.39) and PMSC-2 (DE = 0.51), *i.e.* Fig. 8b and c, a larger pore size ~10 μm prevailed along with thicker walls ~0.5 to 1 μm. This implied a higher volume and stronger support for water loading. Considering the effect of PDMS on strengthening the aforementioned mechanical properties, it provided stronger support for the swollen structure because of the increased thickness and toughness. However, for PMSC-3 (DE = 0.6), Fig. 8d illustrates a different micro-architecture compared to other compositions, with numerous spherical phases distributed within the swollen pores of PMSC-3. With a larger amount of PDMS incorporated, increased hydrophobicity causes a macro-phase separation, which came with a long-range repulsive interaction. This repulsive force mechanically weakened PMSC with increasing brittleness, as depicted by its deteriorated mechanical properties.[31]

In addition, at a swelling ratio of about 250%, the fracture stress and the fracture strain of PMSC-2 reached 252 ± 22.3 kPa and 4.6, respectively. Regarding the sample with an approximate swelling ratio of 1400%, the fracture stress and the fracture strain of PMSC-1, PMSC-2, and PMSC-3 were measured as values of (118 kPa, 3.07), (204 kPa, 5.69), and (162.3 kPa, 2.27), respectively, and the stain–stress curve is shown in Fig. S5b.† Besides, from the results it was shown that PMSC-2 still had a better mechanical strength than the others. Therefore, compared with previous reports on PDMS-grafted chitosan amphiphilic hydrogels, such flexibility was relatively much higher than what has been addressed. It was found that the PDMS-grafted chitosan hydrogels synthesized in the past usually displayed stiffness, with tensile strength and elongation of 1–10 MPa and 0.15–0.3, respectively, but with an equilibrium swelling ratio of <100%.[35–42] This implied that PMSC hydrogels demonstrated much better elasticity and water absorbability compared to all the PDMS-*g*-chitosan hydrogels addressed in the past.

Hence, for the NOCC, the amino and carboxyl groups offer amphoteric and hydrophilic properties, which can accordingly generate a large π_{ion} and π_{mix} to assist water-in diffusion.[32] However, the weaker polymer–polymer interaction provided an inverse π_{elast} that was too small to counteract π_{ion} and π_{mix}. Therefore π_{final} was unable to reach zero, *i.e.* an equilibrium swelling state. By cross-linking with PDMS, increased hydrophobicity and elasticity, together with the decreased number of –COOH groups, produced lower π_{mix}, π_{elast} and π_{ion}, so the PMSC hydrogels can achieve a swelling equilibrium without structural degeneration.

Construction of volume-transition model

Considering the effect of PDMS on the polymer–solvent interaction (π_{mix}), the electrostatic interaction (π_{ion}), and the polymer–polymer interaction (π_{elast}) upon swelling, the model of the volume-phase transition of the PMSC hydrogels can be illustrated in Fig. 9a, which is used to describe the swelling process. In the earlier stage, amphiphilic PMSC hydrogels demonstrated a hierarchical structure, in which compact hydrophobic PDMS-rich aggregates were cross-linked within the underlying network structure. Right after immersing in water, the hydrophobicity reduced π_{mix} to inhibit the water intake. This resistance slowed

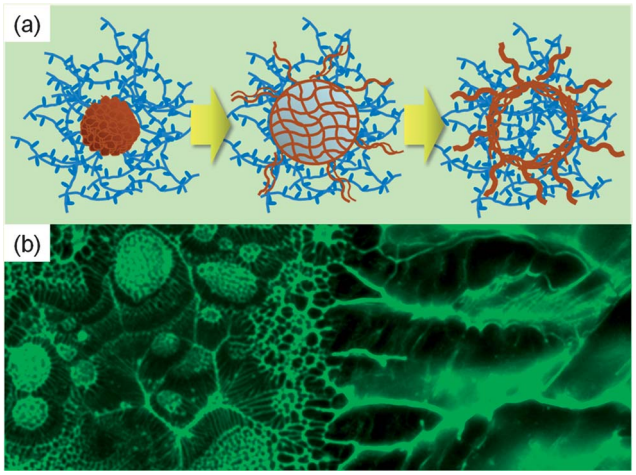

Fig. 9 (a) Schematic model of the swelling process of PMSC hydrogels. The hydrophobic blocks which represent PSMC segments are brown, and the hydrophilic NOCC is blue. (b) Real observation of the hydrogels with different water uptakes by confocal laser microscopy.

down the swelling rate, especially for the hydrophobic part, *i.e.* the spherical microgels. As time passed, hydration and electrostatic interaction evolved between the water and the ionized –COOH groups, and a developing π_{ion} caused a slight separation of adjacent polymer chains. Because π_{ion} is relying upon the presence of –COOH groups, the higher degree of PDMS grafting (which corresponds to a decreased amount of free –COOH groups) decreased the extent of ionization (π_{ion}), resulting in a reduction in the swelling rate of microgels. Moreover, since the relaxation of microgels is dominant in the earlier swelling dynamics, according to the swelling-related process, the response time τ for any application during volume phase transitions of the hydrogels can be correlated to their characteristic dimension length (l),[33]

$$\tau \sim \text{length}^2/D_{coop} \quad (7)$$

where D_{coop} is the cooperative diffusion coefficient. As the size and the number of compact microgels were increased with increasing amount of PDMS, the swelling rate should be dependent on the size and number of microgels. Indeed, the swelling kinetics in Fig. 6a clearly show that with increasing amount of PDMS, the size and the number of aggregation (microgels) increased, which in turn led to longer relaxation times of the networks.

In the later stage, wherein the microgels were completely relaxed, the exposure of the stretched PDMS-rich chains caused a phase separation between water and those hydrophobic polymer segments, resulting in the formation of a macro-metric network, *i.e.*, consisting of bundles of polymer chains (polymer-rich phase, *i.e.* thick wall) and a solvent-rich phase (forming large pores upon swelling). Such a structural development gave rise to higher elasticity, which caused a decrease in π_{elast}. Therefore, the thick and elastic frame constructed a physical barrier, which gave the diffusion limit shown by the n values of 0.382 and 0.331, for PMSC-2 and PMSC-3 in Fig. 6b, respectively, which are beyond the regime of the Fickian diffusion mode ($n = 0.5$). Indeed, by confirming the assumed model, the real observation of the swelling-related process by CLSM is shown in Fig. 9b.

In short, the swelling of this newly synthesized amphiphilic PMSC hydrogel can be explained based on existing mathematical models. The PMSC hydrogels were similar in swelling behavior to those observed in existing superabsorbent polymers (SAPs), which were defined as having the ability to absorb 10–1000 times the amount (based on original weight) of water or aqueous fluids over a relatively short period of time.[34] These newly developed PMSC hydrogels exhibited not only a high swelling ratio, but based on the microphase separation, the cross-linker, PDMS, giving the unique hierarchical structure. Hence, by optimizing PDMS addition, the structural morphology is tunable so that highly efficient water absorbability can be manipulated to meet both the mechanical and practical requirements for numerous advanced applications, including superabsorbents, wound dressings, scaffolding matrix, bio-adhesives, and drug delivery systems.

Conclusions

A novel amphiphilic PMSC CAPN was successfully synthesized, wherein the hydrophobic PDMS segments act not only as a cross-linker to impart an efficient self-foaming capability, but also a mechanical reinforcement to escalate both the strength and elasticity of the resulting hydrogel, upon extensive swelling. Microstructural evolution confirmed swelling by more than 30 times in aqueous solution, with prominent flexibility maintained over a long period of time. A new swelling model based on spectroscopic examination of the hybrid hydrogel was proposed, which nicely described the swelling behavior and also the corresponding microarchitectural development of the hydrogel under extensive solvation. A synergistic combination of both silicone and polysaccharides built in the new type of hydrogel envisions a number of advanced biomedical applications such as wound dressing, scar prevention, artificial skin, smart patches, and a responsive drug delivery system to be practically attainable.

Acknowledgements

This work was financially supported by the National Science Council of the Republic of China, Taiwan under Contract of NSC 100-2320-B-009-006-MY2 and NSC 99-2113-M-009-013-MY2.

Notes and references

1 T. Tanaka, *Gels. Sci. Am.*, 1981, **244**, 110.
2 M. Shibayama and T. Tanaka, *Adv. Polym. Sci.*, 1993, **109**, 1.
3 P. Calvert, *Adv. Mater.*, 2009, **21**, 743.
4 J. A. Johnson, N. J. Turro, J. T. Koberstein and J. E. Mark, *Prog. Polym. Sci.*, 2010, **35**, 332.
5 J. P. Gong, Y. Katsuyama, T. Kurokawa and Y. Osada, *Adv. Mater.*, 2003, **15**, 1155.
6 J. Hu, K. Hiwatashi, T. Kurokawa, S. M. Liang, Z. L. Wu and J. P. Gong, *Macromolecules*, 2011, **44**, 7775.
7 J. S. Boateng, K. H. Matthews, H. N. E. Stevens and G. M. Eccleston, *J. Pharm. Sci.*, 2008, **97**, 2892.
8 J. Klode, L. Schöttler, I. Stoffels, A. Körber, D. Schadendorf and D. J. Dissemond, *J. Eur. Acad. Dermatol. Venereol.*, 2011, **25**, 933.
9 H. Omidian, K. Park and J. G. Rocca, *J. Pharm. Pharmacol.*, 2007, **59**, 317.
10 C. Fodor, G. Kali and B. Ivan, *Macromolecules*, 2011, **44**, 4496.
11 P. Alexandridis, *Curr. Opin. Colloid Interface Sci.*, 1996, **1**, 490.
12 Q. Zhang, S. Zhang and W. Li, *Polymer*, 2011, **52**, 5471.
13 A. Domjan, P. Mezey and J. Varga, *Macromolecules*, 2012, **45**, 1037.
14 R. A. A. Muzzarelli, *Carbohydr. Polym.*, 2009, **76**, 167.
15 X. G. Chen, Z. Wang, W. S. Liu and H. J. Park, *Biomaterials*, 2002, **23**, 4609.
16 M. Momeni, F. Hafezi, H. Rahbar and H. Karimi, *Burns*, 2009, **35**, 70.
17 X. Thomas, Silicones in Industrial Applications: Medical applications, in *Inorganic polymers*, ed. R. D. Jaeger, M. Gleria, Nova Science Publishers, New York, 2007.
18 E. R. Hayes, *US Pat.*, 4619995, 1986.
19 T. Y. Liu, S. Y. Chen, Y. L. Lin and D. M. Liu, *Langmuir*, 2006, **22**, 9740.
20 M. Vamvakaki and C. Patrickios, *J. Phys. Chem. B*, 2001, **105**, 4979.
21 J. Eastoe, in *Colloid Science: Principle, Methods, and Applications*, ed. Cosgrove and Terence, Wiley, 2010, ch. 4 and 5, pp. 61–114.
22 B. Hammouda, D. Ho and S. Kline, *Macromolecules*, 2002, **35**, 8578.
23 K. Jha, R. A. Hule, T. S. Jiao, S. Teller, R. J. Clifton, R. L. Duncan, D. J. Pochan and X. Jia, *Macromolecules*, 2009, **42**, 537.
24 E. Jarkova, N. K. Lee and T. A. Vilgis, *J. Chem. Phys.*, 2003, **119**, 3541.
25 S. C. George and S. Thomas, *Polymer*, 1996, **37**, 5839.
26 A. Richter, G. Paschew, S. Klatt, J. Lienig, K. F. Arndt and H. J. P. Adler, *Sensors*, 2008, **8**, 561.
27 M. J. Owen, *CHEMTECH*, 1981, **11**, 288.
28 ed. R. G. Jones, W. Ando and J. Chojnowski, *Silicon Chemistry*, 2002, vol. 1, p. 309.
29 V. K. Mouryaa, N. N. Inamdara and A. Tiwari, *Adv. Mater. Lett.*, 2010, **1**, 11.
30 T. S. Anirudhan and S. Rijith, *J. Environ. Radioact.*, 2012, **106**, 8.
31 T. Ohta and A. Ito, *Phys. Rev. E: Stat. Phys., Plasmas, Fluids, Relat. Interdiscip. Top.*, 1995, **52**, 5250.
32 R. A. A. Muzzarelli and C. Muzzarelli, *Adv. Polym. Sci.*, 2005, **186**, 151.
33 K. F. Arndt, F. Krahl, S. Richter and G. Steiner, in *Swelling-Related Processes in Hydrogels*, ed. G. Gerlach and K.-F. Arndt, Hydrogel Sensors and Actuators, 2009, pp. 74–100.
34 M. J. Zohuriaan-Mehr and K. Kabiri, *Iran. Polym. J.*, 2008, **17**, 451.
35 D. K. Kweon, *Polym. Bull.*, 1998, **41**, 645.
36 M.-S. Shin, S. I. Kim, I. Y. Kim, N. G. Kim, C. G. Song and S. J. Kim, *J. Appl. Polym. Sci.*, 2002, **84**, 2591.
37 I. Y. Kim, S. J. Kim, M.-S. Shin, Y. M. Lee, D. I. Shin and S. I. Kim, *J. Appl. Polym. Sci.*, 2002, **85**, 2661.
38 M. Rutnakornpituk, P. Ngamdee and P. Phinyocheep, *Carbohydr. Polym.*, 2006, **63**, 229.
39 D. Enescu, V. Hamciuc, L. Pricop, T. Hamaide, V. Harabagiu and B. C. Simionescu, *J. Polym. Res.*, 2009, **16**, 73.
40 D. Enescu, *J. Macromol. Sci., Part A: Pure Appl. Chem.*, 2009, **46**, 438.
41 D. Enescu, V. Hamciuc, R. Ardeleanu, M. Cristea, A. Ioanid, V. Harabagiu and B. C. Simionescu, *Carbohydr. Polym.*, 2009, **76**, 268.
42 N. Rodkate, U. Wichai, B. Boontha and M. Rutnakornpituk, *Carbohydr. Polym.*, 2010, **81**, 617–625.

